Entrainment and deposition of boulders in a gravel bed river

Pascal Allemand[1], Eric Lajeunesse[2], Olivier Devauchelle[2], Vincent J. Langlois[1]

[1]Université Claude Bernard Lyon 1, ENS Lyon, Université Jean Monnet Saint-Étienne & CNRS, Laboratoire de Géologie de Lyon, Terre Planètes Environnement, UMR 5276, 69100 Villeurbanne, France

[2]Université de Paris, Institut de Physique du Globe de Paris, CNRS, F-75005, Paris, France

Correspondence to: Pascal Allemand (allemand@univ-lyon1.fr)

Abstract.

We propose a new method to characterize bedload transport in rivers. Using a drone equipped with a high resolution camera, we recorded yearly images of a bar of the Vieux-Habitants river, a gravel-bed river located on Basse-Terre Island (Guadeloupe, French West Indies). These images, combined with high frequency measurements of the river discharge, allow us to monitor the evolution of the population of boulders on the river bed. Based on this dataset, we estimate the smallest discharge that can move the boulders, and calculate the time during which the river effectively transports them. We find that the transport of boulders occurs for approximately 10 hours per year. When plotted as a function of the effective transport time, the population of boulders that were in place at the beginning of the survey decreases exponentially, with an effective residence time of approximately 17 hours. Based on our results, we suggest a new method to estimate the bedload discharge in gravel bed rivers.

1 Introduction

Rivers collect sediment from the surrounding hillslopes and carry it down to the oceans (Leopold and Emmett, 1976). The resulting sediment flux is often intermittent: only during floods does the river exert a force strong enough to move the sediments of its bed (Phillips and Jerolmack, 2014; Philipps et al., 2018). Flood after flood, a river gradually exports sediment out of its catchment. The frequency of ~~the~~ floods and the quantity of sediment that each of them transports thus set the erosion rate within the catchment (Wolman and Miller, 1960).

The fate of a particle entrained during a flood depends on its size. Fine sediments are carried in suspension. Coarse sediments, conversely, travel as bedload: they roll, slip and bounce on the river bed, until they eventually settle down. This process is inherently stochastic (Einstein, 1937). A turbulent burst or a collision with a travelling grain can dislodge a particle from the bed (Charru et al., 2004; Ancey et al., 2008; Houssais and Lajeunesse, 2012). Once in motion, the particle's velocity fluctuates and its eventual deposition is, again, a random process (Lajeunesse et al., 2010; Furbish et al., 2012). Even in a steady flow, a sediment particle spends most of its time at rest on the bed; its journeys downstream are rare and short events (Lajeunesse et al., 2017). Overall, the combination of these stochastic events generates a downstream discharge of sediment, referred to as

"bedload transport", whose intensity depends on the properties of the flow, and on the ~~grain~~ size, density, and shape of the sediment particles (Einstein, 1950; Bagnold, 1973, 1977).

Bedload transport accounts for a large part of the sediment load exported out of mountainous catchments (Métivier et al., 2004; Meunier et al., 2006; Liu et al., 2008). It carves the channel of bedrock rivers, controls the shape and size of alluvial rivers, and generates ripples, dunes, bars and terraces (Gomez, 1991; Church, 2006; Seminara, 2010; Devauchelle et al., 2010; Aubert et al., 2016; Métivier et al., 2017; Dunne and Jerolmack, 2020; Abramian et al., 2020). In the field, geomorphologists measure bedload by collecting the moving particles in traps or baskets (Helley and Smith, 1971; Leopold and Emmett, 1976; Habersack et al., 2016). These direct measurements are laborious, and sometimes risky. These difficulties have motivated the development of alternative methods. One may, for example, estimate the intensity of bedload transport from the acoustic or seismic noise it generates (Burtin et al., 2008, 2011, 2014; Turowski and Rickenmann, 2009; Mao et al., 2016). However, the calibration of these seismic and acoustic proxies still requires direct measurements (Gimbert et al., 2014; Thorne, 2014; Burtin et al., 2016).

An alternative is to monitor the displacements of individual particles (Dietrich and Smith, 1984). These tracers – painted boulders or Radio Frequency Identification Passive Integrated Transponders (RFID PIT) inserted into the boulder– travel with the flow during floods (Cassel et al., 2020). Between two floods, one may look for the tracers on the exposed river bed. By repeating this procedure, one gradually reveals the trajectories of the tracers. Although laborious, this method provides reliable information, without perturbing the flow. Tracer particles have been used to evaluate the storage of particles in the sediment bed (Haschenburger and Church, 1998; Bradley, 2017), and to estimate the distance that a bedload particle travels before it settles down (Ferguson and Wathen, 1998; Martin et al., 2012). When their number is large, tracers form a plume, which disperses as it travels downstream (Bradley and Tucker, 2012; Phillips and Jerolmack, 2014). One may then infer the mean bedload discharge from the elongation of this plume (Lajeunesse et al., 2018).

Measuring bedload transport, nonetheless, remains arduous, and some questions are still open. On average, how often can a river transport its coarsest sediment? How long does a boulder remain on the river bed? We propose a new approach to address these questions. Instead of tracking the particles when they travel, we monitor the evolution of their population at a fixed location. In that sense, our method can be called "Eulerian". Using a drone, we recorded yearly images of the bed of the Vieux Habitants river (section 2), a gravel-bed river located in Basse-Terre Island (Guadeloupe, French West Indies). Combined with high frequency measurements of the river discharge, these images allow us (1) to follow the population of boulders that make up the bed, (2) to determine the threshold discharge above which the flow puts these boulders into motion (section 3), and (3) to estimate the residence time of boulders in the river bed.

2 Field site, measurement and processing

We conducted our investigation on Basse-Terre Island, a volcanic island of the Guadeloupe archipelago, which is part of the subduction arc of the Lesser Antilles (Feuillet et al., 2002 - Fig. 1a). Basse-Terre's climate is tropical, with daily temperatures

between 24 and 28 °C, and an average rainfall rate of about 5200 mm y^{-1}. Rains occur mainly as short and intense events. During the rainy season, which extends from June to January, storms and hurricanes are frequent, and the rainfall rate may reach up to 590 mm day^{-1}. As a result, the discharge of rivers varies abruptly, with frequent flash floods.

Rad et al. (2006) estimated the erosion rate of several Basse-Terre catchments based on the chemical composition of the dissolved load. They found that it varies between 800 and 4000 t km^{-2} y^{-1}, or, equivalently, 0.3 and 1.5 mm y^{-1} (for a rock density of about 2900 kg m^{-3}). These values are consistent with the volume of sediment mobilized by landslides during extreme climatic events (Allemand et al., 2014). They place Basse-Terre Island amongst the fastest eroding places on Earth (Summerfield and Hulton, 1994). This observation led to the creation of the "Observatoire de l'Eau et de l'éRosion aux Antilles" (ObsERA), an observatory which monitors erosion within the French Network of Critical Zone Observatories (Gaillardet et al., 2018). Our field site is located in the Vieux-Habitants catchment which is monitored by ObsERA.

The Vieux-Habitants river (Fig. 1b) drains a 30 km^2 watershed on the leeward (West) side of the island. Most of the watershed, made of andesitic lava and pyroclastic deposits aged from 600 to 400 ky, is covered with a dense rain forest (Samper et al., 2007). The Vieux-Habitants river flows over 19 km, from its headwater at an altitude of 1300 m, down to the Vieux-Habitants village, where it discharges into the Caribbean Sea. The channel is made of bedrock, partly covered with a thin layer of alluvial sediment. Five kilometers from the sea, the river turns alluvial, and its slope gradually decreases. Our field site is a reach of the Vieux-Habitants river located 3 km from the sea, at an elevation 45 m a.s.l. There, the river bed is alluvial and the channel, meanders between two steep banks about 2.5 m high. A large boulder bar, 300 meters long and 35 meters wide, lies on the inner side of the channel (Fig. 1c, d).

The *Direction de l'Environnement, de l'Aménagement et du Logement* (DEAL-Guadeloupe) operates a stream gauge, at the Barthole station, three kilometers upstream of our field site (Fig. 1b). This station has been measuring the river discharge every ten minutes for more than 15 years, except for an interruption between 2009 and 2011. As no major tributary joins the main stream between Barthole and our field site, we shall assume that the data acquired in Barthole provides a reasonable estimate of the river discharge at our site.

The data acquired between 2011 and 2018 reveals that the discharge stays below 10 m^3 s^{-1} for 91% of the time (Fig. 2a). In this low flow state, the boulder bar emerges and the river flows in a channel that forms between the bar and the left bank of the river (Fig. 1d). There, the water depth is about 0.3 m, but may locally exceed 0.7 m (Fig. 1c, d). Floods are characterized by a steady increase of the discharge during 1 to 6 hours, followed by a recession that lasts typically 4 to 18 hours (Fig. 2b - Guérin et al., 2018). The largest flood ever recorded in Barthole occurred during hurricane Maria, from September 18 to September 19, 2017. The water discharge then reached more than 250 m^3 s^{-1}, flooding not only the bar but also the river's banks. After the hurricane, the river returned to its normal course, along the left side of the bar.

To understand how floods affect the river's bed, we acquired aerial images of our field site with an uncrewed hexacopter Aerial Vehicle named DRELIO (for *DRone hELIcoptère pour l'Observation de l'environnement*). This device, specially designed

for tropical conditions, is capable of flying in steep, densely vegetated watersheds, and requires only a small takeoff area (Delacourt et al., 2009). It carries a high resolution camera. We started working in 2011, with a Nikon D700 reflex camera, equipped with a 35 mm lens. In 2016, we replaced it with a Sony Alpha 7 reflex, still in use at present. As a result, the resolution of our images improved from 0.04 meters/pixel in 2011 to 0.02 meters/pixel starting from 2016.

From 2011 to 2018, we performed 8 field campaigns following the same procedure. We flew DRELIO at an elevation of 80 m above the river bed, and used the on-board camera to acquire a series of images that covered the entire boulder bar with an 30% overlap between two neighboring images. Using the MicMac Photogrammetric suite (Rupnik et al., 2017), we computed for each campaign a Digital Surface Model (DSM) and an orthoimage of the bar. An orthoimage is an image from which the distortion due to relief has been suppressed. Two georeferenced orthoimages of the same surface can be superimposed. Each orthoimage is georeferenced using fixed ground control points, whose coordinates are measured by Differential Global Navigation Positioning System. The resolution of the orthoimages ranges from 0.04 m to 0.02 m depending on the acquisition year. However, the georeferencing is not perfect and the series of diachronic orthoimages do not exactly overlap. We selected the 2012 orthoimage as a base image on which we warped the other orthoimages. We then draw the contour of the boulders visible on each orthoimage using a raster graphic editor. The diameter of the smallest visible grains is at least 5 pixels (0.1 to 0.15 m). On the bar, however, most boulders have a diameter larger than 0.2 meters, and some are larger than 1 meter (Terry and Goff, 2014). In practice, we restrict our analysis to boulders with a diameter larger than 0.5 meters, as they are clearly distinguishable on the images. Using an open-source Geographical Information System software (QGis), we vectorize the contours of these boulders and calculate their exposed area, A, from which we deduce the boulder equivalent diameter, defined as the diameter D of a disk with the same surface area, $D = 2\sqrt{A/\pi}$. The error on the surface is between 15 and 20 % for the smaller diameters. With this method, we obtain 8 diachronic superimposable orthoimages and 8 vector files of the boulders shapes, position and equivalent diameter.

Figure 3 shows a close view of two orthoimages, in the region of the bar delineated by the red rectangle in Fig. 1d. The first orthoimage was acquired in March 2012 (Fig. 3, left) and the second one in June 2013 (Fig. 3, right). In both cases, the flow in the river was low, and the water level, partly visible in the upper part of the images, was about the same. The comparison between these two orthoimages reveals some changes at the surface of the bar. Several boulders (yellow contours on Fig. 3), lying on the bar in 2012, are not visible anymore in 2013: they were entrained downstream by the river, sometime between our two acquisition campaigns. Conversely, we also observe, in 2013, ~~s~~several boulders that were not present in 2012 (red contours on Fig. 3): these boulders must have been deposited on the bar, sometime between the two images. Finally, the rest of the boulders (blue contours on Fig. 3) remained in place. The comparison between two consecutive GIS therefore allows us to identify the fate of each boulder. Based on this method, we attribute to each boulder of each image, a label which specifies whether the boulder was already in place during the previous campaign, or if it was deposited recently. Some cases turn out to be ambiguous: a few boulders disappeared and then reappeared on more recent images, as floods covered them with sediment, before exposing them again. Those ambiguous cases were duly labelled and the corresponding boulders were considered

immobile. Following this procedure, we end up with a dataset that contains the position and the size of all the boulders larger than 0.5 m. We also know whether each of them stayed in place or whether, and when, it was deposited or entrained away. In short, we have turned the boulders into tracers. In the next section, we use this dataset to characterize the transport of boulders in the Vieux-Habitants river.

3 Results

3.1 Structure of the bar: mobile and consolidated layers

Our data show that entrained and deposited boulders are uniformly distributed over the whole bar. There is no particular place from which boulders were preferentially exported, nor onto which they were preferentially deposited. This suggests that, during floods, bedload transport is uniform over the bar.

Our dataset also reveals the existence of two families of immobile boulders. The first one corresponds to boulders that were deposited on the bar during the course of our survey, and remained immobile for several years, until the river entrained them again. The second one corresponds to boulders that remained immobile during the whole survey. The latter are partially buried in a matrix of smaller sediment and appear to belong to a stable underlying base layer, that spans over the entire bar. These observations are consistent with the concept of active layer (e.g. Church and Haschenburger, 2006). We therefore interpret them as the result of the existence of two layers of boulders: (i) an active surface layer of mobile boulders, and (ii) an underlying basal layer of static ones. Interestingly, laboratory experiments report a similar division between an active layer of mobile grains, that regularly settle on the bed until the flow eventually dislodges them and set them back in motion, and a layer of static grains (Charru et al., 2004, Lajeunesse et al., 2010). In the following, we focus on the properties of the layer of mobile boulders.

3.2 Granulometric distribution

We start our analysis by focusing on the motion of boulders of size between 0.5 and 2 meters. To characterize their distribution, we divide this interval into six 0.25 m-wide bins, and distribute the boulders in each one, according to their equivalent diameter. We then compute the dimensionless surface density of each class *i*, defined as the number of grains per unit surface, normalized by the area of a grain:

$$\tilde{\sigma}_i = \frac{N_i \times \pi D_i^2}{S} \quad (1)$$

where N_i is the number of boulders in class *i*, D_i is their equivalent diameter, and S=2000 m^2 is the area of the bar. The dimensionless surface density σ_i can also be interpreted as the proportion of the bar area occupied by the boulders of class *i*.

The number of boulders in each class and the corresponding surface density vary from year to year. To account for these variations, we compute these two quantities for each field campaign, and represent the results in the form of a box plot (Fig.

4a). We find that the surface density of each class varies by less than 27% around its median value. The size distribution of the boulders thus does not change significantly with time, but appears to be roughly at equilibrium. This equilibrium is not static, but dynamic. Indeed, distinguishing the boulders freshly deposited (Fig. 4a, green boxes) from those that were already in place during the preceding campaign (Fig. 4a, yellow boxes) shows that about half of the population of boulders is renewed each year (Fig. 4a). In short, the number of boulders entrained by floods balances, on average, the number of fresh boulders deposited on the bar, thus maintaining constant their surface density (Fig. 4b).

Finally, our analysis shows that the surface density rapidly decreases with grain size (Fig. 4a). With a surface density $\sigma = 0.23$ boulders m^{-2}, or equivalently, a total number of about 350 boulders over the 2000 m2 of the bar, boulders of size 0.5 to 0.75 m dominate the bar, at least in the range of diameters accessible to our measurement. The transport rate of these boulders is also sufficiently high to allow for significant statistics. In the following, we shall therefore focus on the transport of boulders of size 0.5 to 0.75 m. Before we do so, however, we first need to evaluate the threshold discharge above which these boulders are set in motion. This is the topic of the next section.

3.3 Threshold for the initiation of transport

Based on our dataset, we can identify the largest boulders deposited on, or entrained from, the bar between two consecutive campaigns. Plotting their diameter as a function of the maximum water discharge between two campaigns, we find that the size of these boulders increases with the maximum discharge (Fig. 5). Assuming that the largest boulders are transported when the discharge is at its highest, the resulting curve provides a reasonable estimate of the threshold discharge beyond which grains of a given size are entrained by the flow. For lack of sufficient data, however, we cannot estimate the threshold discharge of boulders smaller than 0.5 m. Instead, we shall now try to evaluate it, by extrapolating from our observations.

In practice, the threshold discharge corresponds to the discharge for which the shear stress exerted by the river on its bed exceeds a critical value (Shields, 1936). The instantaneous turbulent stress exerted on the river bed is, however, highly variable in space and in time: it depends on the flow, on the shape of the channel, on the river slope, on the bed roughness, and its measurement in the field is challenging (Henderson 1963, Parker 1978, Chauvet et al., 2014, Métivier et al., 2017, Nezu and Nakagawa, 1993). Here, to simplify the problem, we assimilate the river to a rectangular channel of width *W*, depth *H*, and slope *S*. Based on the Darcy-Weisbach equation, we then derive the threshold discharge required to transport a boulder (see appendix for a full derivation):

$$Q_c = W \frac{D^{3/2}}{S} \left(\Theta_c \frac{\Delta\rho}{\rho} \right)^{3/2} \left(\frac{g}{C_f} \right)^{1/2} \quad (2)$$

where $\Delta\rho = \rho_s - \rho$ is the difference between the density of rock and that of water, C_f is the Darcy-Weisbach friction parameter, g is the acceleration of gravity, and Θ_c is the threshold Shields parameter (Shields, 1936). Our model is crude and some of the parameters in equation (2) are difficult to estimate. Based on direct field measurements, we estimate the river width to be W=30 m. Using the DEM, we calculate its average slope and find it to be about S = 0.03. For the friction coefficient, we use

the value $C_f = 0.1$, typical of mountain streams (Limerinos, 1970). A fit of equation (2) to our data reasonably accounts for our observations (Fig. 5), and yields a threshold Shields stress θ_c=0.032, which falls in a realistic range (Buffington and Montgomery, 1997; Lamb et al.,2008).

Encouraged by this result, we use equation (2) to calculate the threshold discharge of the boulders of size 0.5 to 0.75 m. We find a threshold discharge between 24 and 69 m^3s^{-1}, with a value of 45 m^3s^{-1} for the intermediate Shields number of 0.032. In the next section, we use this value to estimate the time during which the river effectively transports these boulders.

3.4 Effective transport time

Boulders of size 0.5 to 0.75m move only when the river discharge exceeds the threshold value of 45 m^3s^{-1} calculated in the previous section. Their effective transport time is therefore the cumulated time that the river spends above this threshold (Fig. 6). We find that it amounts to a total of 85 hours for the period 2011 to 2018. The time fraction during which the river is above the entrainment threshold is thus I= 0.12%. This means that, on average, boulders can move during about 10 hours each year.

The effective transport time depends on the occurrence of floods, and therefore, on the distribution of rainfalls. As the latter varies from year to year, so does the effective transport time (Fig. 6): the river spent less than 5 hours above 45 m^3s^{-1} between 2014 and 2016 (an unusually dry period). Conversely, it spent 32 hours above 45 m^3s^{-1} between 2017 and 2018, a period that includes hurricane Maria. Even during those years, the annual effective transport time did not exceed 0.36% of the year that is about 30 hours. On a tropical volcanic island like Guadeloupe, ~~the~~ boulders move only during short periods of time, whose cumulated duration depends on the frequency and the intensity of the storms.

3.5 Evolution of the population of boulders

So far, we have focused on the threshold of transport and the effective transport time of boulders. We now use our data to document the evolution of their population. As in previous sections, we restrict our analysis to boulders of size 0.5 to 0.75m. We start by identifying all the boulders lying on the bar in 2011. Using our dataset, we then monitor the evolution of this population. We find that its number decreases with the effective transport time, as boulders are progressively entrained by floods, and replaced with new ones (Fig. 7), an observation similar to those of Wilcock and McArdell (1997) and Harchenbucher and Wilcock (2003).

Repeating the same procedure with the boulders lying on the bar in 2012, and the following years until 2017,we end up monitoring a total of seven populations of boulders. To compare their evolution, we normalize the number of boulders in each population with its initial value, and plot the result as function of the effective transport time (Fig. 7). We find that all data points gather around the same trend: the number of boulders decreases rapidly at first. With time, however, the rate gradually slows down.

As the surface density of boulders is small (σ =0.23 boulder m^{-2} - see section 3.2), we expect little interaction between them during transport. Following Einstein (1937) and Charru et al. (2004), we thus assume that the number of boulders that leave the bar is proportional to the number of boulders available on its surface, that is:

$$\frac{dN}{dt} = -\frac{N}{\tau} \quad (3)$$

where t is the effective transport time, N is the number of boulders on the bar surface at time t, and τ is a characteristic entrainment time. The solution of Eq. (3), $N = N_0 e^{-t/\tau}$, is a decaying exponential, of characteristic time τ, where N_0 is the initial number of boulders. Fitting this exponential solution to our data yields a good representation of the evolution of N (R^2 =0.84). We find a characteristic time τ =17 hours (Fig. 7).

The model proposed here is simplistic. It does not take into account the variations of discharge during a flood, and relies on a crude description of the threshold of transport. Yet, the exponential decrease of an initial population of boulders is consistent with the data plotted on figure 7, and we therefore expect that the value of the characteristic time τ is a reasonable estimate of the residence time of boulders on the bar, expressed in terms of the effective sediment transport time. This residence time is short. Expressed in terms of half-life, it takes an effective transport time of log2 τ = 12 hours to entrain half of the boulders initially present on the bar, and to replace them with new ones.

4. Discussion - Conclusion

To the best of our knowledge, we present the first attempt at characterizing bedload transport based on yearly UAV image acquisition. Despite — or, maybe, owing to — its simplicity, the method proves robust: the comparison of images taken one year apart allowed us to monitor the evolution of the population of boulders at the surface of the Vieux-Habitants river. Using high frequency measurements of the river discharge, we determine the threshold discharge necessary to set boulders in motion, and estimate the time during which the flow is strong enough to transport them. The model of threshold we use, despite its simplicity, reproduces well our observations for a realistic range of parameters.

In the Vieux-Habitants river, this effective transport time amounts to 10.5 hours per year on average, that is about I=0.12% of the time. The transport of boulders is therefore a rare event controlled by the occurrence of floods, which, in its turn, depends on the distribution of rainfalls. A change of this distribution is likely to impact the quantity of sediment transported by the river.

Einstein (1937) was the first to propose that the entrainment of bedload particles is inherently a random process. This hypothesis is at the core of the entrainment-deposition model (Charru et al., 2004; Lajeunesse et al., 2010; 2018). When expressed in terms of the effective transport time, our data are consistent with this assumption: the population of boulders on the bed of the Vieux-Habitants river decreases exponentially, as expected for a random Poisson process. The characteristic time of this decay — in fact, the residence time of the boulders on the bed — is short: τ =17 hours of effective transport time.

We suggest a method to estimate the sedimentary discharge associated to boulder transport, based on the exponential decay of a population of well-identified boulders. During a flood, entrained boulders will travel over a distance L_f that depends on the duration and on the intensity of the flood. The discharge of boulders across a given section of the river is the number of grains entrained per unit time, from a bed area of size WL_f. The boulder discharge is therefore the total number of boulders at rest on this surface, $\sigma W L_f$, divided by the residence time, τ, where σ is the surface density of boulders (Einstein, 1937). The instantaneous volumetric discharge is then the number of grains entrained by unit time, times the average volume of grains. To convert this value into an annual sediment flux, we multiply it by the proportion of time, *I*, during which the river is above the entrainment threshold. L_f is the most difficult parameter to estimate. It can be approached by using a tranport law (Lajeunesse et al., 2010) or measured in the field using RFID tracers as proposed by Phillips and Jerolmack (2014).

Code/Data availability

Discharge data used for figures 2 and 6 are available on http://www.hydro.eaufrance.fr/. UAV Images and dataset are available on Harvard Dataverse https://dataverse.harvard.edu/dataset.xhtml?persistentId=doi:10.7910/DVN/QRHM8E

Author contributions

PA designed and performed the field measurements, and processed the resulting data. All authors developed the overall ideas and were responsible for critical contributions, passing the final manuscript and editing text and figures.

Competing interests.

The authors declare no competing interests.

Acknowledgements

This work was carried out in the framework of Obsera (Observatoire de l'Eau et de l'Erosion aux Antilles). Obsera is part of OZCAR infrastructure. P. Grandjean, S. Passot, V. Robert et T. Kitou are warmly thanked for their efficiency and involvement in this work. This is IPGP contribution n°

Appendix A - Threshold discharge

Here, we estimate the threshold discharge above which the river can transport its sediment. To do so, we assimilate the channel to a rectangle of width W, depth H, and slope S. The Darcy-Weisbach equation then relates the average flow velocity V to the shear stress τ exerted on the river bed (Limerinos, 1970):

$$\tau = C_f \rho V^2 \quad \text{(A1)}$$

where ρ is the density of water and C_f is the Darcy-Weisbach friction coefficient. In steady state, the momentum balance requires that:

$$\tau = \rho g S H. \quad \text{(A2)}$$

At the onset of sediment motion, the Shield number, Θ, defined as the ratio between the driving force acting on the grains and the weight of a grain, must equal a threshold value Θ_c:

$$\Theta = \frac{\tau}{\Delta \rho g D} = \Theta_c, \quad \text{(A3)}$$

where Δρ is the difference between the density of a grain and that of water, g, is the acceleration of gravity, and D is the grain size. Combining (A2) with (A3) yields the expression of the flow depth H at the threshold of entrainment:

$$H = \Theta_c \frac{\Delta \rho}{\rho} \frac{D}{S}. \quad \text{(A4)}$$

Similarly, combining (A1) with (A2) and (A3) yields the average flow velocity at the threshold of entrainment:

$$V = \left(\Theta_c \frac{\Delta \rho}{\rho} \frac{g D}{C_f} \right)^{1/2}. \quad \text{(A5)}$$

Injecting the velocity and the flow depth into the expression of the water discharge, $Q = WHV$, we find the threshold discharge above which the river can transport a boulder of diameter D:

$$Q_c = W \frac{D^{3/2}}{S} \left(\Theta_c \frac{\Delta \rho}{\rho} \right)^{3/2} \left(\frac{g}{C_f} \right)^{1/2} \quad \text{(A7)}$$

This expression, of course, is only a crude estimate, if only because the river is not a straight rectangular channel. Nonetheless, it provides a decent approximation of the flow conditions that are necessary to initiate the transport of a given class of boulders (Figure 5).

References

Abramian, A., Devauchelle, O., and Lajeunesse, E.: Laboratory rivers adjust their shape to sediment transport, Physical Review E, 102, 053101, doi: 10.1103/PhysRevE.102.053101, 2020.

Allemand, P., Delacourt, C., Lajeunesse, E., Devauchel, O., and Beauducel, F.: Erosive effects of the storm Helena (1963) on Basse Terre Island (Guadeloupe — Lesser Antilles Arc), Geomorphology, doi: 10.1016/j.geomorph.2013.09.020, 2014.

Ancey, C., Davison, A., Bohm, T., Jodeau, M., and Frey, P.: Entrainment and motion of coarse particles in a shallow water stream down a steep slope, J. Fluid Mech., 595, 83–114, doi: 10.1017/S0022112007008 774, 2008.

Aubert, G., Langlois, V.J., Allemand, P.: Bedrock incision by bedload: insights from direct numerical simulations, Earth Surf. Dynam., 4, 327–342, doi: 10.5194/esurf-4-327-2016, 2016.

Bagnold, R.: The nature of saltation and of Bedload transport in water, Proc. R. Soc. Lond., A 332, 473–504, 1973.

Bagnold, R.: Bedload transport by natural rivers, Water Resources Research, 13, 303–312, 1977.

Bradley, D. N.: Direct Observation of Heavy-Tailed Storage Times of Bedload Tracer Particles Causing Anomalous Superdiffusion, Geophysical Research Letters, 44, doi: 10.1002/2017GL075045, 2017.

Bradley, D. N. and Tucker, G. E.: Measuring gravel transport and dispersion in a mountain river using passive radio tracers, Earth Surface Processes and Landforms, 37, 1034–1045, doi: 10.1002/esp.3223, 2012.

Buffington, J., and Montgomery, D.: A systematic analysis of eight decades of incipient motion studies, with special reference to gravelbedded rivers, Water Resour. Res., 33, 1993–2029, doi: 10.1029/97WR03138, 1997.

Burtin, A., Bollinger, L., Vergne, J., Cattin, R., and Nábelek, J.: Spectral analysis of seismic noise induced by rivers: A new tool to monitor spatiotemporal changes in stream hydrodynamics, Journal of Geophysical Research: Solid Earth, 113, doi: 10.1029/2007JB005034, 2008.

Burtin, A., Cattin, R., Bollinger, L., Vergne, J., Steer, P., Robert, A., Findling, N., and Tiberi, C.: Towards the hydrologic and bedload monitoring from high-frequency seismic noise in a braided river: The “torrent de St Pierre”, French Alps, Journal of hydrology, 408, 43–53, doi: 10.1016/j.jhydrol.2011.07.014, 2011.

Burtin, A., Hovius, N., McArdell, B., Turowski, J., and Vergne, J.: Seismic constraints on dynamic links between geomorphic processes and routing of sediment in a steep mountain catchment, Earth Surf. Dynam., 2, 21–33, doi: 10.5194/esurf-2-21-2014, 2014, 2014.

Burtin, A., Hovius, N., and Turowski, J. M.: Seismic monitoring of torrential and fluvial processes, Earth Surf. Dynam., 4, 285–307, doi: 10.5194/esurf-4-285-2016, 2016.

Cassel, M., Piegay, H., Fantino, G., Lejot, J., Bultingaire, L., Michel, K. and Perret, F.: Comparison of ground-based and UAV a-UHF artificial tracer mobility monitoring methods on a braided river, Earth Surf. Process. Landforms, 5, 1123-1140, doi: 10.1002/esp.4777, 2020.

Charru, F., Mouilleron, H., and Eiff, O.: Erosion and deposition of particles on a bed shared by a viscous flow, Journal of Fluid Mech., 519, 55–80, doi:10.1017/S0022112004001028, 2004.

Chauvet, H., Devauchelle, O., Métivier, F., Lajeunesse, E., and Limare, A.: Recirculation cells in a wide channel, Phys. Fluids, 26, 016604, 1–10, doi: 10.1063/1.4862442 2014.

Church, M.: Bed material transport and the morphology of alluvial river channels, Annu. Rev. Earth Planet. Sci., 34, 325–354, doi: 10.1146/annurev.earth.33.092203.122721, 2006.

Church, M., and Haschenburger, J.K.: What is the "Active Layer"? Water Resour. Res. 2017, 53, 5–10, doi: 10.1002/2016WR019675, 2017.

Delacourt, C., Allemand, P., Jaud, M., Grandjean, P., Deschamps, A., Ammann, J., Cuq, V., and Suanez, S.: DRELIO: An unmanned helicopter for imaging coastal areas, SI 56, Proceedings of the 10th International Coastal Symposium), 1489-1493, Lisbon, Portugal, 2009.

Devauchelle, O., Malverti, L., Lajeunesse, E., Lagrée, P., Josserand, C., and Thu-Lam, K.: Stability of bedforms in laminar flows with free surface: from bars to ripples, Journal of Fluid Mechanics, 642, 329–348, doi: 10.1017/S0022112009991790, 2010.

Dietrich,W. and Smith, J.: Bedload Transport in a River Meander, Water Resources Research, 20, doi: 10.1029/WR020i010p01355, 1984.

Dunne, K. B. and Jerolmack, D. J.: What sets river width? Science advances, 6, doi: 10.1126/sciadv.abc1505, 2020.

Einstein, H.: The bed-load function for sediment transportation in open channel flows, US Department of Agriculture. Soil Conservation Service, 1950.

Einstein, H. A.: Bedload transport as a probability problem, in: Sedimentation: 746 Symposium to Honor Professor H.A. Einstein, 1972. translation from 747 German of H.A. Einstein doctoral thesis. Originally presented to Federal Institute of Technology, Zurich, Switzerland, 1937, pp. C1 – C105, 1937.

Ferguson, R. and Wathen, S.: Tracer-pebble movement along a concave river profile: Virtual velocity in relation to grain size and shear stress, Water Resources Research, 34, 2031–2038, doi: 10.1029/98WR01283, 1998.

Feuillet, N., Manighetti, I., and Tapponnier, P.: Arc parallel extension and localization of volcanic complexes in Guadeloupe, Lesser Antilles. J. Geophys. Res., 107, 1-29, doi: 10.1029/2001JB000308, 2002.

Furbish, D., Roseberry, J., and Schmeeckle, M.: A probabilistic description of the bedload sediment flux: 3. The particle velocity distribution and the diffusive flux, Journal of Geophysical Research, 117, F03 033, doi: 10.1029/2012JF002356, 2012.

Gaillardet, J., I. Braud, F. Hankard, S. Anquetin, O. Bour, N. Dorfliger, et al.: OZCAR: The French network of critical zone observatories. Vadose Zone J. 17:180067, doi: 10.2136/vzj2018.04.0067, 2018.

Gimbert, F., Tsai, V. C., and Lamb, M. P.: A physical model for seismic noise generation by turbulent flow in rivers, J. Geophys. Res. Earth Surf., 119, 2209–2238, doi: 10.1002/2014JF003201, 2014.

Gomez, B.: Bedload transport, Earth-Science Reviews, 31, 89–132, doi: 10.1016/0012-8252(91)90017-A, 1991.

Guerin, A., Devauchelle, O., Robert, V., Kitou, T., Dessert, C., Quiquerez, A., et al.: Stream-discharge surges generated by groundwater flow. Geophysical Research Letters, 46, 7447–7455. doi:10.1029/2019GL082291, 2019.

Habersack, H., Kreisler A., Rindler R., Aigner J., Seitz, H., Liedermann, M., Laronne, J.B.: Integrated automatic and continuous bedload monitoring in gravel bed rivers, Geomorphology, doi: 10.1016/j.geomorph.2016.10.020, 2016.

Haschenburger, J.K. and Church, M.: Bed material transport estimated from the virtual velocity of sediment. Earth Surf. Process. Landforms, 23: 791-808. doi: 10.1002/(SICI)1096-9837(199809)23:9<791::AID-ESP888>3.0.CO;2-X, 1998.

Haschenburger, J. K. and Wilcock, P.R.: Partial transport in a natural gravel bed channel. Water Resources Research, 39, 1, 1020, doi: 10.1029/2002WR001532, 2003.

Helley, E.J. and Smith, W.: Development and calibration of a pressure-difference bedload sampler, Geological Survey Open-File Report, December 3, 1971., 1971.

Henderson, F. M.: Stability of alluvial channels, T. Am. Soc. Civ.Eng., 128, 657–686, 1963.

Houssais, M. and Lajeunesse, E.: Bedload transport of a bimodal sediment bed, J. Geophys. Res., 117, F04015, doi: 10.1029/2012JF002490, 2012.

Lajeunesse, E., Malverti, L., and Charru, F.: Bedload transport in turbulent flow at the grain scale: experiments and modeling, J. Geophys. Res, 115, F04 001, doi: 10.1029/2009JF001 628, 2010.

Lajeunesse, E., Devauchelle, O., Lachaussée, F., and Claudin, P.: Bedload transport in laboratory rivers: the erosion-deposition model, in: Gravel-bed Rivers: Gravel Bed Rivers and Disasters, Wiley-Blackwell, Oxford, UK, 415–438, doi: 10.1002/9781118971437.ch15, 2017.

Lajeunesse, E., Devauchelle, O., and James, F.: Advection and dispersion of bed load tracers, Earth Surf. Dynam., 6, 389–399, doi: 10.5194/esurf-6-389-2018, 2018.

Lamb, M.P., Dietrich, W.E., and Venditti, J.G.: Is the critical Shields stress for incipient sediment motion dependent on channel-bed slope? J. Geophys. Res., 113, F02008, doi:10.1029/2007JF000831, 2008.

Leopold, L. B. and Emmett, W. W.: Bedload measurements, East 85 Fork River, Wyoming, Proceedings of the National Academy of Sciences, 73, 1000–1004, 1976.

Limerinos, J.T.: Determination of the Manning coefficient from measured bed roughness in natural channels. United States, Geological Survey, Water-Supply Paper 1898-B, 1970.

Liu, Y., Metivier, F., Lajeunesse, E., Lancien, P., Narteau, C., and Meunier, P.: Measuring bedload in gravel bed mountain rivers: Averaging methods and sampling strategies, Geodin. Acta, 21, 81–92, doi: 10.3166/ga.21.81-92, 2008.

Mao, L., Carrillo R, Escauriaza C, Iroume A.: Flume and field-based calibration of surrogate sensors for monitoring bedload transport. Geomorphology, 253, 10–21. doi: 10.1016/j.geomorph.2015.10.002, 2016.

Martin, R. L., Jerolmack, D. J., and Schumer, R.: The physical basis for anomalous diffusion in bedload transport, Journal of Geophysical Research, 117, F01 018, doi: 10.1029/2011JF002075, 2012.

Métivier, F., Meunier, P., Moreira, M., Crave, A., Chaduteau, C., Ye,B., and Liu, G.: Transport dynamics and morphology of a high mountain stream during the peak flow season: The ürümqi River (Chinese Tianshan), in River Flow 2004: Proceedings of the Second International Conference on Fluvial Hydraulics, edited by M. Greco et al., pp. 761– 777, Taylor and Francis, Philadelphia, Pa.

Métivier, F., Lajeunesse, E., and Devauchelle, O.: Laboratory rivers: Lacey's law, threshold theory, and channel stability, Earth Surf. Dynam., 5, 187–198, doi: 10.5194/esurf-5-187-2017, 2017.

Meunier, P., Metivier, F., Lajeunesse, E., Meriaux, A.S., and Faure, J.: Flow pattern and sediment transport in a braided river: The “torrent de St Pierre” (French Alps), J. Hydrol., 330, 496–505, doi: 10.1016/j.jhydrol.2006.04.009, 2006.

Nezu, I and Nakagawa, H.: Turbulence in Open Channel Flows. IAHR Monograph, A. A. Balkema, Rotterdam, 1993.

Parker, G.: Self-formed straight rivers with equilibrium banks and mobile bed. Part 1. The sand-silt river, J. Fluid Mech., 89, 109–125, 1978.

Phillips, C. B. and Jerolmack, D. J.: Dynamics and mechanics of bed-load tracer particles, Earth Surf. Dynam., 2, 513–530, doi: 10.5194/esurf-2-513-2014, 2014.

Phillips, C., Hill, K. M., Paola, C., Singer, M., and Jerolmack, D.:Effect of flood hydrograph duration, magnitude, and shape on bed load transport dynamics, Geophys. Res. Lett., 45, 8264–8271, doi: 10.1029/2018GL078976, 2018

Rad, S., Louvat, P., Gorge, C., Gaillardet, J., and Allègre, C.J.: River dissolved and solid loads in the Lesser Antilles: new insight into basalt weathering processes. J. Geochem. Explor. 88, 308-312, doi: 10.1016/j.gexplo.2005.08.063, 2006.

Rupnik, E., Daakir, M., Deseilligny, M.P.: Open Geospatial Data, Software and Standards 2:14, doi:10.1186/s40965-017-0027, 2017.

Samper, A., Quidelleur, X., Lahitte, P., and Mollex, D.: 2007. Timing of effusive volcanism and collapse events within an oceanic arc island: Basse-Terre, Guadeloupe archipelago (Lesser Antilles Arc). Earth Planet. Sci. Lett. 258, 175–191, doi:10.1016/j.epsl.2007.03.030, 2007.

Seminara, G.: Fluvial sedimentary patterns, Annual Review of Fluid Mechanics, 42, 43–66, doi: 10.1146/annurev-fluid-121108-145612, 2010.

Shields, A. S.: Anwendung der Aehnlichkeitsmechanik und der Turbulenzforschung auf die Geschiebebewegung, Mitteilung der Preussischen Versuchsanstalt fur Wasserbau und Schiffbau, 26, 1936.

Summerfield, M. A., and Hulton, N. J.: Natural controls of fluvial denudation rates in major world drainage basins, J. Geophys. Res., 99(B7), 13871–13883, doi: 10.1029/94JB00715, 1994.

Terry, J.P., and Goff, J.: Megaclasts: proposed revised nomenclature at the coarse end of the Udden-Wentworth grain-size scale for sedimentary particles, Journal of Sedimentary Research, 84 (3): 192–197, doi: 10.2110/jsr.2014.19, 2014.

Thorne, P. D.: An overview of underwater sound generated by interparticle collisions and its application to the measurements of coarse sediment bedload transport, Earth Surf. Dynam., 2, 531–543, doi: 10.5194/esurf-2-531-2014, 2014.

Turowski, J. M. and Rickenmann, D.: Tools and cover effects in bedload transport observations in the Pitzbach, Austria. Earth Surf. Process. Landforms, 34: 26-37. doi: 10.1002/esp.1686, 2009.

Wilcock, P.R. and McArdell, B.W.: Partial transport of a sand/gravel sediment. Water Resources Research, 33, 235-245, doi: 10.1029/96WR02672. 1997.

Wolman, M. G. and Miller, J. P.: Magnitude and frequency of forces in geomorphic processes, The Journal of Geology, 68, 54–74, 1960.

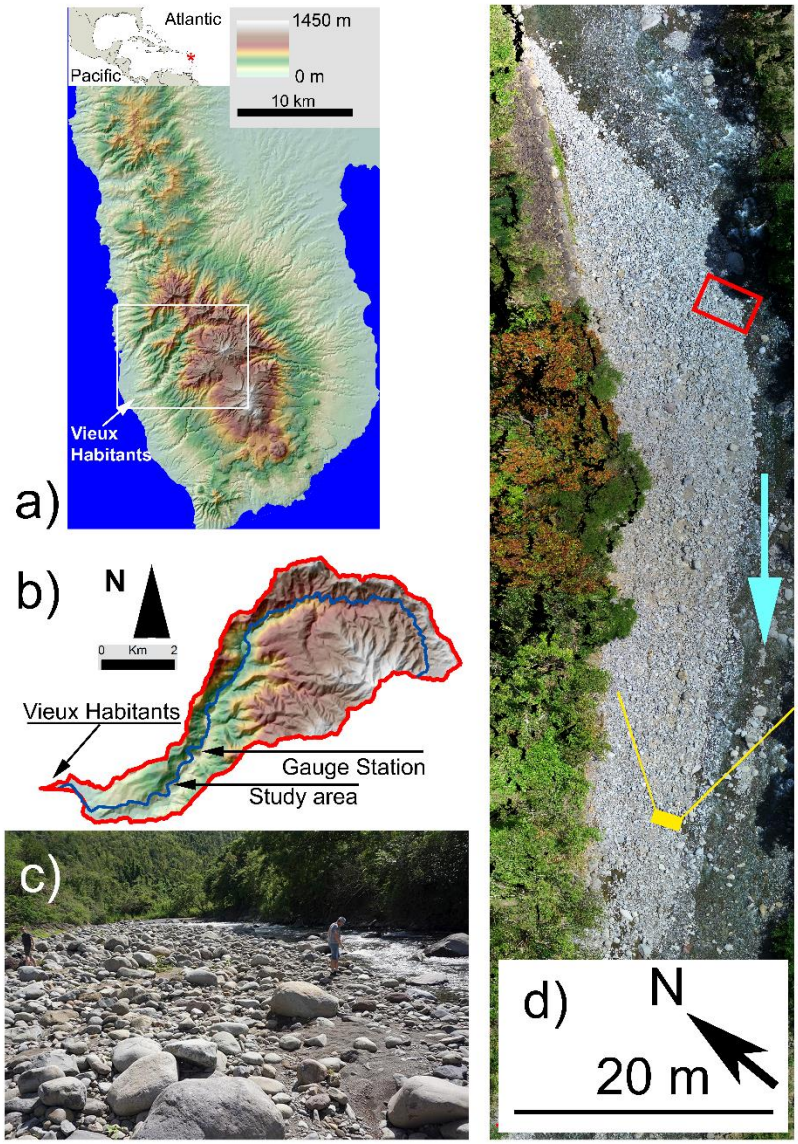

Figure 1: a) Basse Terre island in the Guadeloupe archipelago. The island separates the Atlantic Ocean in the East from the Caribbean Sea in the West. The white rectangle shows the position of the map displayed in b). b) The Vieux-Habitants river is located on the Caribbean side of Basse Terre. The watershed of Vieux-Habitants has an area of 19 km^2. The length of the river is 19 km. The water discharge is measured each 10 minutes at Barthole gauge station. The study area is located 2 km downstream of Barthole. c) A view of the bar from ground looking upstream shows the size of the boulders and their heterometric distribution. The two persons give the scale. d) The area of interest. The bar is about 300 m long and 15 to 35 m wide. It lies on the right side of the river 3 km upstream of the seashore. In fair weather conditions, the bar is bounded on its left by the channel of the river which is 5 to 10 m wide and less than 1 m deep. The boulder bar is flooded 1 to 3 times a year. The red square shows the location of Fig. 3. The position of the camera and the field of view of c) is shown in yellow. The flow direction is given by the turquoise arrow.

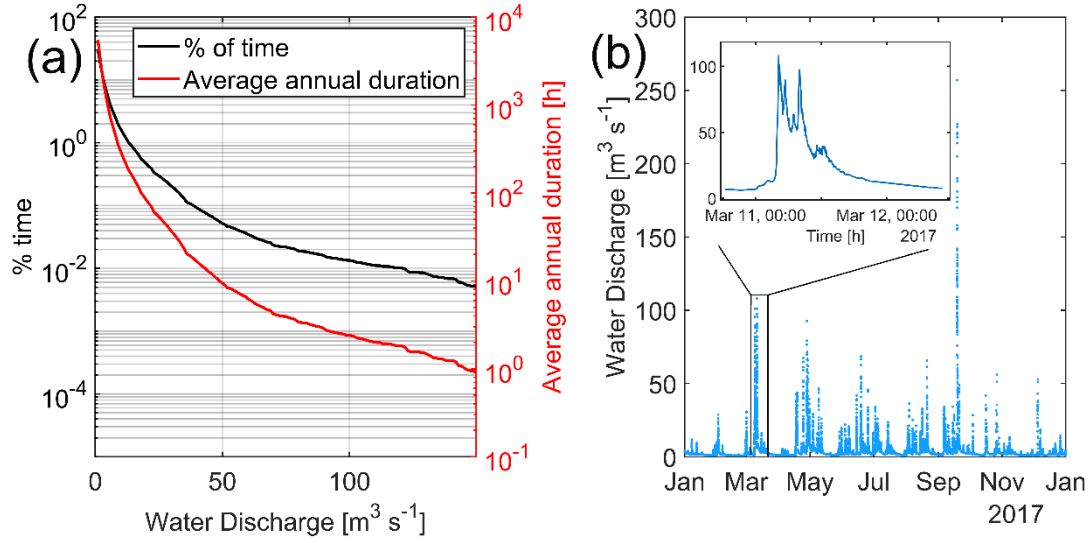

435 **Figure 2:** a) Percentage of time during which the water discharge is above a given threshold based on data from 2011 to 2018. b) Hydrograph of year 2017. Most of the time, river is in low flow conditions with less than 5 m^3s^{-1}. The largest recorded discharge was 263 $m^3 s^{-1}$. It was reached on September 19 2017 during hurricane Maria. c) The inset shows a typical flood. The water discharge reaches its maximum in less than one hour. The peak of the flow is followed by a slow recession.

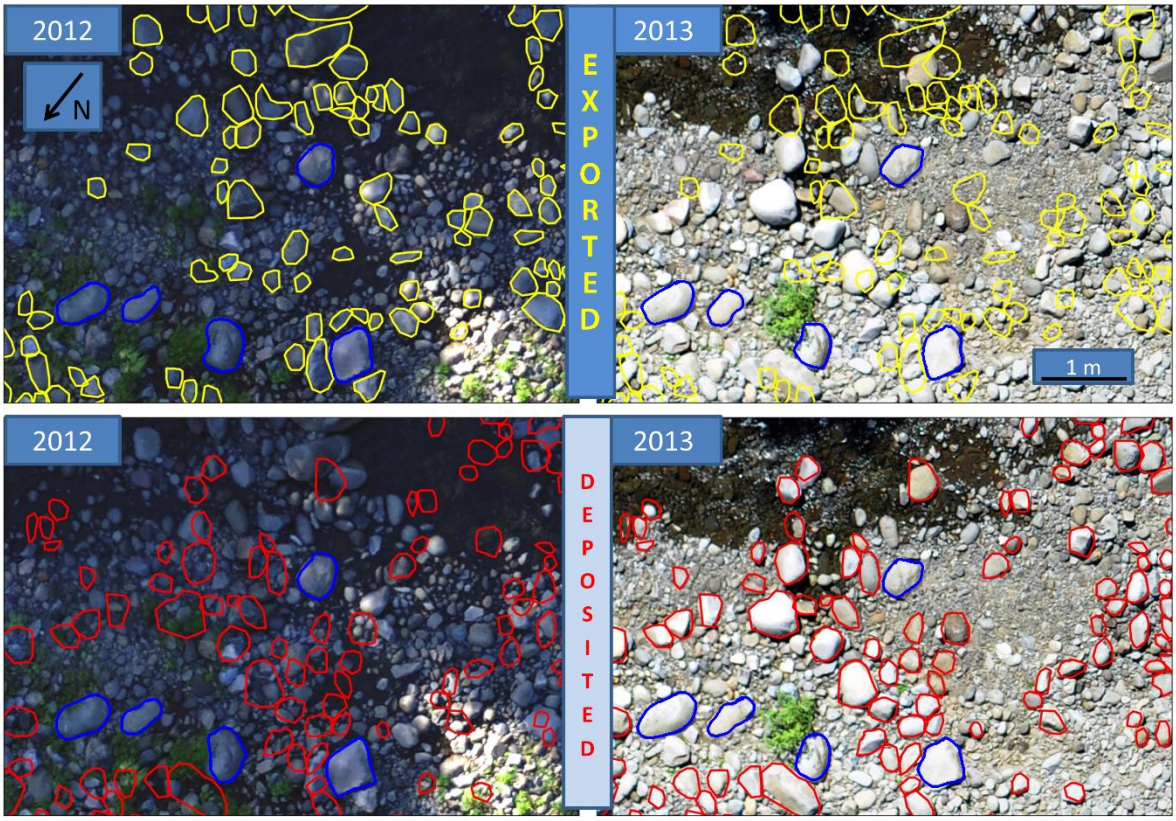

Figure 3: Comparison between the surface of the bar in March 2012 (left) and June 2013 (right). The upper pictures show the boulders that moved between 2012 and 2013. The lower pictures show the boulders that were deposited during the same period. Some boulders, outlined in blue, visible in 2012 are still there in 2013.

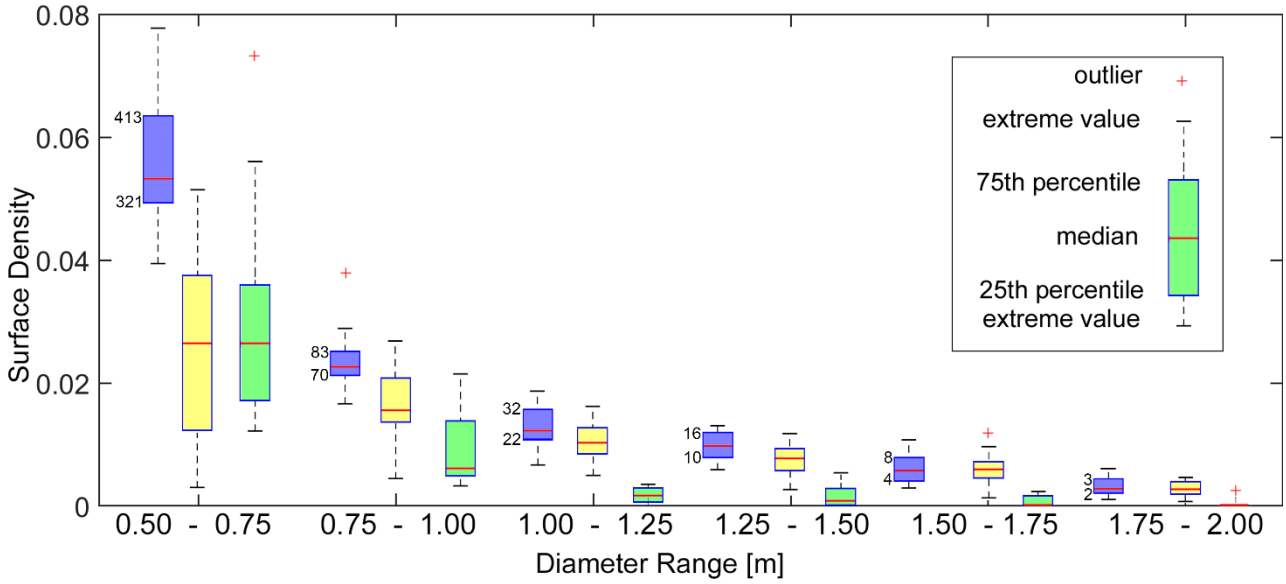

Figure 4a: Box plot of the surface boulder density (Eq. 1) on the bar as a function of the boulder diameter computed for the whole duration of our survey. Blue: total number of boulders; green: freshly deposited boulders; yellow: boulders that were already in place during the preceding campaign of observation.

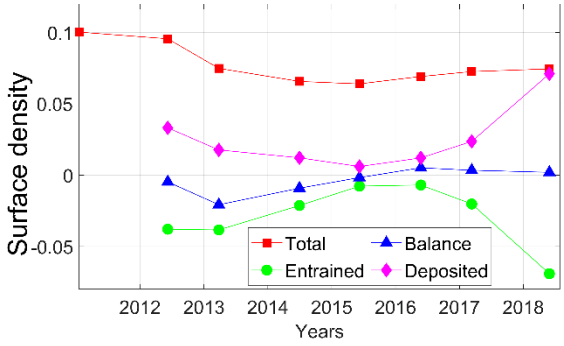

Figure 4b: b) Surface density of entrained, deposited and total boulder population Data from 2010 have been obtained from a preliminary campaign.

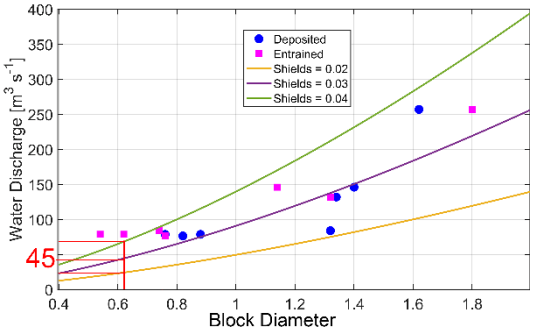

Figure 5: Maximum discharge recorded at the gauge station as a function of the size of the largest transported boulders from 2011 to 2018. The curves represent the theoretical relation between water discharge and the maximum diameter of the exported or deposited boulders given by Eq. (2) (Appendix 1) for 3 values of Shields stress. The threshold discharge for boulders with a diameter of 0.625 m ranges from 24 to 69 $m^3 s^{-1}$ According to the Shields stress. The parameters used for the theoretical estimation of the flow threshold are: Darcy-Weisbach friction coefficient C_f=0.1, critical Shield number Θ_c= 0.02-0.04, width of river, W=30 m, Δρ the density difference between grains and water 1900 kg m^{-3}.

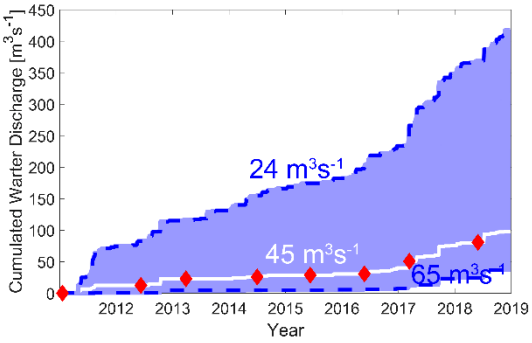

Figure 6: Duration of water discharge between 25 and 64 m^3s^{-1}. The white line represents a water discharge of 45 m^3s^{-1}. Transport is possible only a few hours each year, even during a hurricane year such as 2017. From 2014 to 2016, the transport time was less than 5 hours per year for a threshold of 45 m^3s^{-1}. The red diamonds indicate drone campaigns.

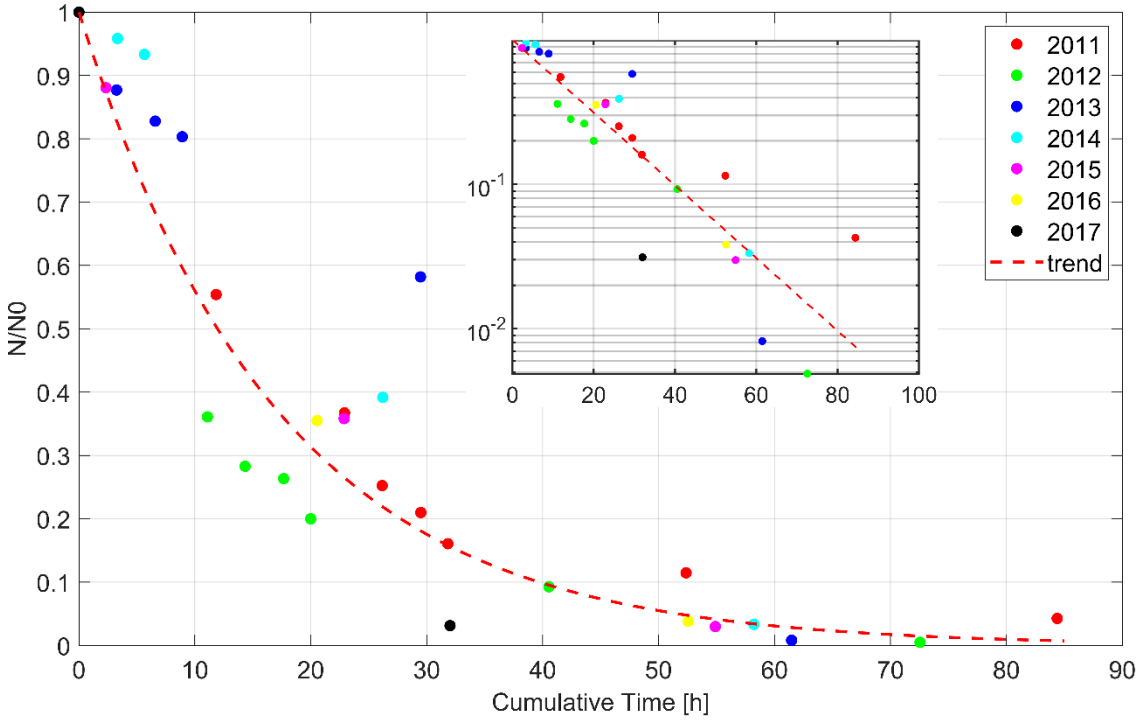

Figure 7: Evolution of the number of boulders deposited on the bar between each campaign, and gradually entrained later. The horizontal axis is the transport time for a discharge threshold of 45 $m^3 h^{-1}$. The red curve is the best fit of Eq. 3 (exponential decay) with a residence time of 17h (half-life of 12 h). Inset: same data in a semi-logarithmic scale.